

Spin Transfer of Quantum Information between Majorana Modes and a Resonator

Alexey A. Kovalev,^{1,2} Amrit De,¹ and Kirill Shtengel¹

¹*Department of Physics & Astronomy, University of California, Riverside, California 92521, USA*

²*Department of Physics & Astronomy, University of Nebraska-Lincoln, Lincoln, NE 68588, USA*

(Dated: November 10, 2021)

We show that resonant coupling and entanglement between a mechanical resonator and majorana bound states can be achieved via spin currents in a 1D quantum wire with strong spin-orbit interactions. The bound states induced by vibrating and stationary magnets can hybridize thus resulting in spin-current induced 4π -periodic torque, as a function of the relative field angle, acting on the resonator. We study the feasibility of detecting and manipulating majorana bound states with the use of magnetic resonance force microscopy techniques.

PACS numbers:

Introduction. — Majorana zero states bound to domain walls in 1D and quasi-1D systems such as p -wave superconducting wires [1], edges of 2D topological insulators [2, 3] and semiconducting quantum wires with strong spin-orbit interactions [4, 5] can be potentially utilized to form non-local qubits thus providing a platform for topological quantum computing [6–8]. Of these systems, spin-orbit-coupled semiconductor wires with proximity-induced superconductivity are of particular interest, with a number of recent experiments aiming at establishing the existence of Majorana bound states (MBS) there [9–12]. While further studies are needed to unambiguously confirm their existence [13–18], one can also look ahead and try developing efficient techniques for manipulating MBS [19–25]. Several recent proposals addressed the possibility of control of topological qubits by coupling them to more conventional ones, such as flux qubits via the Aharonov–Casher effect [26–30].

Proposals related to observation of MBS quite often rely on tunneling and transport effects that are indicative of the zero energy nature of these modes [13–18]. Some recent proposals are also related to unconventional Josephson effect in Majorana quantum wires and TI edges where the periodicity is equal to 4π [1, 4, 31, 32]. A dual effect whereby a torque between magnets exhibits 4π periodicity in the field orientations has also been suggested [33–35]. It is this effect that can lead to mechanical torques and quantum information transfer between MBS and a mechanical resonator. The idea of coupling a two-level system to vibrational modes to form a hybrid quantum system has been successfully used in quantum optics [36] and, more recently, in the field of nanomechanical resonators where a single phonon control has been demonstrated [37]. We propose using a similar technique in the context of topological qubits.

It has been predicted that conservation of angular momentum in macrospin molecules can result in quantum entanglement of a tunneling spin with mechanical modes [38, 39]. A flow of spin current between two magnets has been demonstrated to induce spin-transfer torque effect [40, 41] and mechanical torques [42, 43], also by conser-

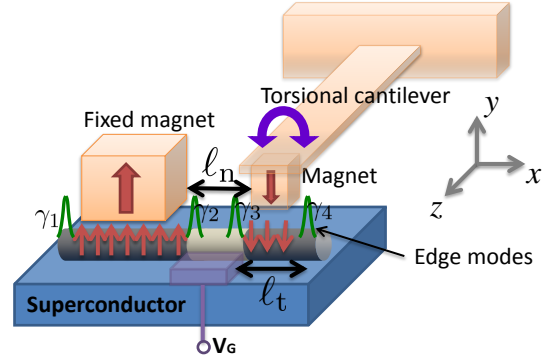


Figure 1: (Color online) A 1D semiconductor wire with strong spin orbit interaction is placed on top of s-wave superconductor. Majorana bound states are defined by magnetic fields of two magnets, one of which is free to vibrate. The gate V_G can be used in order to control the hybridization.

vation of angular momentum. In this Letter, we study resonant coupling between a Majorana qubit and a mechanical resonator induced by spin currents flowing over portions (region of length ℓ_n in Fig. 1) of 1D semiconductor quantum wire. This resonant coupling is controlled by non-dissipative spin currents in a spin-transistor type architecture [44] – which effectively allows or disallows the hybridization of two MBS. A nano-magnet attached to the resonator then feels the hybridization as a mechanical torque which can result in the state (quantum information) transfer between the Majorana qubit and the mechanical resonator.

A Majorana qubit is formed by four MBS where three of these MBS are hybridized (Fig. 1). The non-topological region could be formed by magnets with sharp field profiles or by hetero-junction nanowires with contrasting g -factors. The effective low energy Hamiltonian then becomes:

$$\mathcal{H} = \hbar\omega_r a^\dagger a + iE^n(\theta)\gamma_2\gamma_3 + iE^t\gamma_3\gamma_4, \quad (1)$$

where a is the annihilation operator of the resonant torsional mode of the cantilever so that $\theta = \theta_0 + \theta_{\text{zpt}}(a^\dagger + a)$

with $\theta_{\text{zpf}} = (\hbar^2/KI)^{1/4}$ being the angle of zero point fluctuations of the cantilever, K is the spring constant, I is the moment of inertia, $E^{(n)}$ describes the hybridization energy, γ_i describes MBS. It is the θ dependence of the hybridization energy that leads to three interrelated effects: (i) coupling of the rotation of the magnet to the internal state of Majorana qubit, (ii) mechanical torque acting on the magnets and (iii) spin current $j_s^z(x) = \Re[\Psi^\dagger(x)\hat{\sigma}^z\hat{v}\Psi(x)]$ defined in the non-topological middle section in which the magnetic field is absent, here the velocity operator is $\hat{v} = \partial\hat{H}/\partial p$. We obtain that the torque on the magnets [33–35] is generated solely by the spin current passing through the middle non-topological region when there is no hybridization over the topological regions in Fig 1.

According to our estimates, strong coupling between the Majorana qubit and the mechanical resonator can lead to a shift in the mechanical resonant frequency, Rabi oscillations, coherent state transfer and entanglement. All these effects could signify a presence of a Majorana qubit. This mechanism can also be utilized to couple several Majorana qubits or to couple a Majorana qubit with a non-topological qubit such as an NV center [45].

Spin currents and edge hybridization. — We consider a semiconductor wire with strong spin-orbit interaction in the presence of a Zeeman field (note that a TI edge gives qualitatively similar results). The wire is proximity-coupled to an s -wave superconductor which induces the pairing strength Δ in the wire. A topological region is induced by external magnets (Fig. 1) where one of the magnets is attached to a mechanical resonator and can mechanically vibrate at frequency $\omega_r \ll \Delta$.

The 1D wire is described by a BdG Hamiltonian:

$$\hat{H} = p^2\hat{\tau}^z/2m^* + \alpha_{\text{so}}k\hat{\tau}^z\hat{\sigma}^z - \mu\hat{\tau}^z + \Delta(\cos\phi\hat{\tau}^x - \sin\phi\hat{\tau}^y) - b\hat{\sigma}^z + B(\cos\theta\hat{\sigma}^x - \sin\theta\hat{\sigma}^y), \quad (2)$$

where m^* is the effective mass, α_{so} is the strength of spin-orbit interaction, μ is the chemical potential, $\Delta e^{i\phi}$ is the superconducting pairing, b is the magnetic field along the z -direction and B is the magnetic field in the xy -plane. Here we use the Nambu spinor basis $\Psi^T = (\psi_\uparrow, \psi_\downarrow, \psi_\uparrow^\dagger, -\psi_\downarrow^\dagger)$ and the Pauli matrices $\hat{\sigma}^i$ and $\hat{\tau}^i$ describe the spin and particle-hole sectors, respectively.

The Hamiltonian (2) supports both gapped and gapless phases, its phase diagram is more complicated compared to the TI edge system [33, 34] whose Hamiltonian does not contain the $p^2\tau^z$ term. Here we restrict ourselves to the case $\Delta^2 > b^2$ so that the Hamiltonian (2) describes two gapped phases: topological (T) if $\Delta^2 - b^2 < B^2 - \mu^2$ and non-topological (N) if $\Delta^2 - b^2 > B^2 - \mu^2$, separated by a quantum phase transition at $\Delta^2 - b^2 = B^2 - \mu^2$.

We analyze analytically hybridization of the edge modes which results in spin currents and torques in N–T–N and T–N–T setups shown in Fig. 2 where we have an infinite semiconductor wire with a finite topological (T)

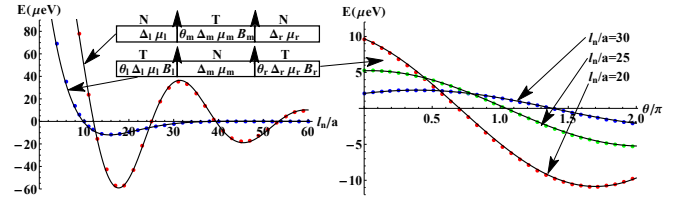


Figure 2: (Color online) Hybridization energies of two Majorana bound states over topological and non-topological regions in a semiconductor wire as a function of the hybridization region length (left) and relative angle of magnetic fields (right), only for T–N–T structures. The circles represent the corresponding numerical results.

or non-topological (N) region. We assume that the phase of the superconducting pairing is constant throughout the wire, the magnetic field is always zero for N-regions and $b = 0$ in all regions. Then gapped regions are described by parameters $\{\Delta, B, \mu, \theta\}$ for the T-region and by $\{\Delta, \mu\}$ for the N-region (see Figs. 2). We first determine the bound state of a single T–N boundary by finding 4-component zero energy solution to the Hamiltonian (2) in the form $\Psi(x) = e^{\kappa x}\Psi(\kappa)$. In general, we arrive at four solutions that decay into the topological region, i.e. with $\Re(\kappa) > 0$, and four solutions that decay into the non-topological region, i.e. with $\Re(\kappa) < 0$. A linear combination of these solutions on each side has to be continuous and have a continuous derivative at the boundary between T and N-regions leading to a unique solution for MBS. We denote such normalized solutions as $|\psi_L\rangle$ for the left Majorana and as $|\psi_R\rangle$ for the right Majorana in Fig. 2. We can use the lowest order perturbation theory to find the hybridization energy of MBS provided that normalized solutions for the left and right edges weakly overlap, i.e. $E^{(n)} \approx |\langle\psi_L|H|\psi_R\rangle|$ where the index stands for the hybridization energy over the non-topological (topological) region. For a T–N–T system in Fig. 2, we obtain the hybridization energy over the non-topological region:

$$\frac{E^n}{E_0^n} \approx e^{-\ell_n \Re(\kappa_2^n)} \cos \left[\frac{\theta}{2} + \Phi_0 + \ell_n \Im(\kappa_2^n) \right], \quad (3)$$

where $\kappa_2^n = m^*/\hbar^2 (i\alpha_{\text{so}} - i\sqrt{2(i\Delta + \mu)\hbar^2/m^* + \alpha_{\text{so}}^2})$, E_0^n and Φ_0 depend on parameters of the T and N-regions and do not depend on ℓ_n and θ [46]. For the spin current we obtain:

$$j_s^z = \pm \frac{\partial E^n(\theta)}{\partial \theta},$$

which shows that the torque $\partial E^n(\theta)/\partial \theta$ acting on the magnets in Fig. 1 is generated solely by the spin current passing through the middle N-region [46]. For N–T–N system in Fig. 2, we obtain the hybridization energy over

the topological region:

$$\frac{E^t}{E_0^t} \approx e^{-\ell_t \kappa_2^t} + |A_0| e^{-\ell_t \Re(\kappa_1^t)} \cos [\arg A_0 + \ell_t \Im(\kappa_1^t)], \quad (4)$$

where κ_1^t and κ_2^t are solutions of equation $\sqrt{B^2 - [\kappa^2(\hbar^2/2m)^2 + \mu]^2} = \Delta + \alpha_{\text{so}}\kappa$ satisfying the condition $\Re(\kappa) > 0$, E_0^t and A_0 depend on parameters of the T and N-regions and do not depend on ℓ_t and θ [46].

Fig. 2 shows the hybridization energies given by Eqs. (3) and (4) for parameters corresponding to an InSb nanowire. We observe an exponential decay with separation and a 4π -periodic behavior with the relative angle of magnetic fields, which is typical for TI edges [33, 34]. In addition, we find an oscillatory behavior of energy as a function of separation between the MBS. Such behavior has been predicted for MBS localized in vortices in 2D p -wave superconductors [47], yet it remained unclear whether these oscillations would persist over a non-topological region. In fact, the absence of oscillations was suggested in [48] but the regime considered there corresponded to a fully depleted electron band.

Numerical results. — We map the BdG Hamiltonian (2) to a tight binding model:

$$\begin{aligned} H = & \sum_{i,\sigma,\sigma'} \left[c_{i+1\sigma}^\dagger (-t_0 \sigma_0 + i \frac{\alpha_i}{2} \sigma_z)_{\sigma\sigma'} c_{i\sigma'} + H.c. \right] \\ & + \sum_{i,\sigma} (2t_0 - \mu_i) c_{i\sigma}^\dagger c_{i\sigma} + \sum_i (\tilde{\Delta}_i c_{i\uparrow}^\dagger c_{i\downarrow}^\dagger + H.c.) \quad (5) \\ & + \sum_i (\tilde{B}_i c_{i\uparrow}^\dagger c_{i\downarrow} + H.c.), \end{aligned}$$

where we introduce complex parameters $\tilde{\Delta} = \Delta e^{i\phi}$ and $\tilde{B} = B e^{i\theta}$. In the long wavelength limit, the tight binding model in Eq. (5) can be reduced to Eq. (2) with $t_0 = \hbar^2/2m^*a^2$, $\alpha = \alpha_{\text{so}}/a$ where a is the lattice constant. For Fig. 2, we use parameters consistent with InSb quantum wires [9], i.e. $m^* = 0.015m_e$, $\alpha_{\text{so}} = 0.2 \text{ eV}\text{\AA}$, $a = 15 \text{ nm}$, $\Delta = 0.5 \text{ meV}$ and $g\mu_B = 1.5 \text{ meV/T}$. The overall length of the wire corresponding to Fig. 1 is 500 sites. Results of our numerical diagonalization of Hamiltonian (5) are presented in Fig. 2 by circles. We observe perfect agreement with analytical Eqs. (3) and (4) when T-regions are formed by uniform magnetic fields.

In Fig. 3(a) and (b) we study the hybridization of MBS that are defined by the modulation of the g -factor (by a factor of 30) in GaSb-GaAs-GaSb type-II nanowire heterostructures [49–51]. Employment of such nanostructures can partially relax the requirement for the sharpness of magnetic field profiles. Due to the bottom of the conduction band mismatch a finite gate voltage is necessary in order to hybridize MBS. In order to study the effect of non-uniform magnetic fields, in Fig. 3(c) the wire is subjected to a constant magnetic field on one half and a field of magnetic dipole at distance h on the other

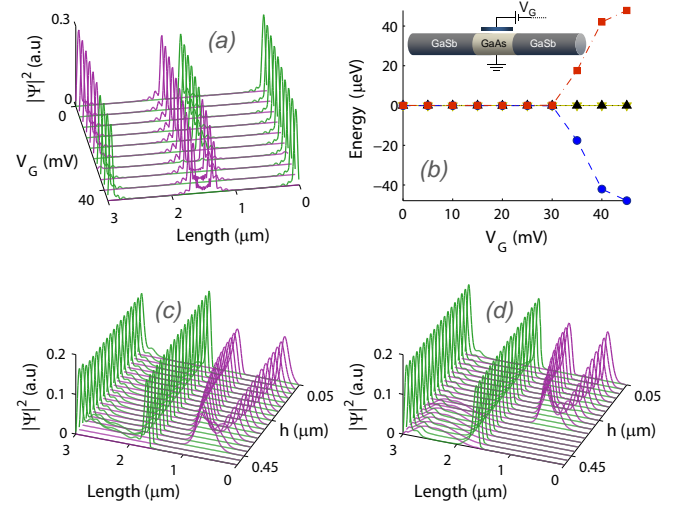


Figure 3: (Color online) (a) We plot edge modes as a function of position and hetero-junction bias voltage V_G , and (b) the corresponding energies as a function of V_G . We see hybridization at $V_G = 30 \text{ meV}$. (c) The wire is subjected to a constant magnetic field on one half and a field of magnetic dipole at distance h on the other half. (d) The same but for a magnetic disk of radius $R = 100 \text{ nm}$ instead of dipole.

half. Somewhat sharper MBS are formed when instead of a dipole we use a perpendicularly magnetized thin disk in Fig. 3(d). The magnetic field decay length along the wire is defined by the distance h between the wire and the magnet in Fig. 1 which implies the requirement $\ell_n \gtrsim h$.

Dissipative dynamics. — We suppose that the section of the wire separating MBS γ_1 and γ_2 is sufficiently long (see Fig. 1). The effective low energy theory describing coupled dynamics of MBS and a mechanical resonator can be described to the lowest order by Hamiltonian in Eq. (1). Without loss of generality, we assume that the electron parity in the wire is 1 which defines the available Hilbert space of two fermions $b_1 = \gamma_1 + i\gamma_2$ and $b_2 = \gamma_3 + i\gamma_4$, i.e. $\alpha|1,0\rangle + \beta|0,1\rangle$. By rewriting Eq. (1) through fermionic operators b_1 and b_2 , and expanding energies around θ_0 , we arrive at the matrix Hamiltonian:

$$\mathcal{H} = \hbar\omega_r a^\dagger a + \left[\frac{E^n(\theta_0)}{4} + \frac{\partial E^n}{\partial \theta} \frac{\theta_{\text{zpf}}}{4} (a^\dagger + a) \right] \sigma_x + \frac{E^t}{4} \sigma_z, \quad (6)$$

where E^n and E^t are given by Eqs. (3) and (4). By tuning either $E^n(\theta_0)/2$ or $E^t/2$ to coincide with $\hbar\omega_r$ (see Fig. 2), we can achieve different regimes of Rabi oscillations. Note that when $\langle \psi_L | H | \psi_R \rangle$ is not pure imaginary we recover additional terms proportional to σ_y in Eq. (6). Here, we analyze the case in which $\hbar\omega_r = E^t/2$ and $E^n(\theta_0) = 0$. From Eq. (3) the coupling strength (Rabi oscillations frequency) is

$$g = \frac{1}{8} \theta_{\text{zpf}} E_0^n e^{-\ell_n \Re(\kappa_2^n)},$$

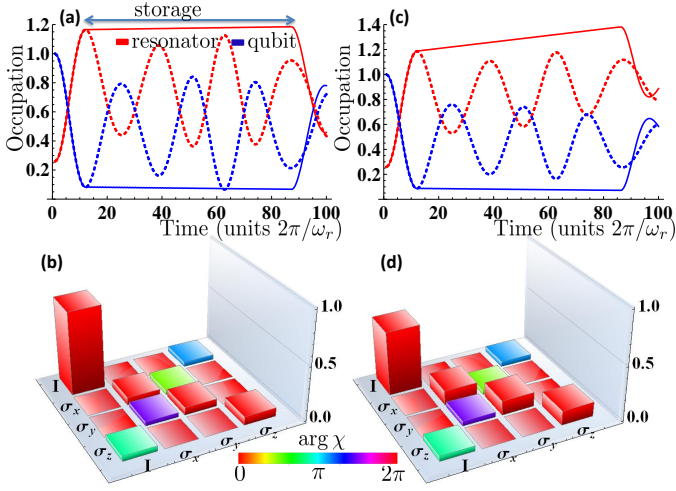


Figure 4: (Color online) (a) Rabi oscillations of a Majorana qubit coupled to a mechanical resonator in Fig. 1. (b) The quantum process tomography of a process in which qubit state is transferred to the resonator, then stored in the resonator while the systems are detuned, and finally transferred back to the qubit. (c) and (d) same as (a) and (b) but for a resonator with smaller quality factor.

which shows that by taking smaller ℓ_n we can increase the coupling strength. The strong coupling regime can be realized when $\omega_r/Q < g$ where Q is the quality factor of the cantilever. A pendulum based on single-walled carbon nanotube with an attached magnet of the size $60 \times 40 \times 20 \text{ nm}^3$ can have $K = 3 \times 10^{-18} \text{ Nm}$ per radian and $I = 4 \times 10^{-34} \text{ kg}\cdot\text{m}^2$ [52]. If we take the corresponding $\theta_{\text{zpf}} = 5 \times 10^{-5}$, $\omega_r = 5 \text{ MHz}$ and $\ell_n = 300 \text{ nm}$ (see Fig. 2) we obtain $g = 100 \text{ kHz}$ which is a strong coupling, e.g. a mechanical resonator with a resonant frequency $\omega_r = 5 \text{ MHz}$ will have to have relatively small $Q > 50$ in order to be in the strong coupling regime. In order to be able to switch off interactions between the Majorana qubit and the resonator one can use special ℓ_t points at which the hybridization energy is close to zero (see Fig. 2). In principle, ℓ_t can be controlled by electrostatic gates [19] or supercurrents [25].

The time dependent dissipative dynamics of the Hamiltonian (6) can be adequately simulated using the Lindblad master equation [53]:

$$\dot{\rho}(t) = -\frac{i}{\hbar} [H(t), \rho] + \frac{1}{2} \sum_k \left[\mathcal{L}_k, \rho(t) \mathcal{L}_k^\dagger \right] + \left[\mathcal{L}_k \rho(t), \mathcal{L}_k^\dagger \right], \quad (7)$$

where we assume that all requirements on the environment for the validity of this approximation apply. Here, \mathcal{L}_k are Lindblad operators, in particular $\mathcal{L}_1 = \sqrt{1/T_1} \sigma_-$ and $\mathcal{L}_2 = \sqrt{1/T_\phi} \sigma_+ \sigma_-$ correspond to the majorana qubit coupling to the environment, $\mathcal{L}_3 = \sqrt{(\bar{n}_r + 1)\omega_r/Q} a$ and $\mathcal{L}_4 = \sqrt{\bar{n}_r \omega_r/Q} a^\dagger$ correspond to the dissipation of the resonator where $\bar{n}_r = [\exp(\omega_r/k_B T) - 1]^{-1}$ and the qubit lifetimes are given by T_1 and $1/T_2 = 1/2T_1 + 1/T_\phi$.

The Majorana qubit can decohere due to tunnelling of fermions in the presence of an external environment such as phonons, two-level systems, classical noise [54], as well as quasiparticle poisoning [55]. As T_1 and T_2 times can strongly depend on the concrete realization, in our simple analysis we choose decoherence times that are order of the magnitude consistent with the above mentioned mechanisms ($T_1 = 70 \mu\text{s}$, $T_2 = 90 \mu\text{s}$).

We present numerical solutions of Eq. (7) for different resonator quality factors, i.e. for $Q = 10^6$ in Figs. 4(a) and (b), and for $Q = 10^5$ in Figs. 4(c) and (d). We assume the resonator temperature $T = 10 \text{ mK}$ and the initial occupation number $\bar{n}_r = 0.26$, e.g. as a result of sideband cooling [56]. Dotted lines represent the Rabi oscillations while the bold lines represent the process in which the Majorana qubit is repeatedly tuned in and out of resonance with the resonator. In such a process the qubit state is transferred from the qubit to the resonator, then stored in the resonator while the systems are detuned, and finally transferred back to the qubit. We can completely describe the process of storage by the quantum process tomography in which the final density matrix of the qubit is described by the process matrix χ , such that $\rho_{\text{out}} = \sum \chi_{i,j} \sigma_i \rho_{\text{in}} \sigma_j$, here σ_j are Pauli matrices and σ_0 is the identity matrix. In Figs. 4(b) and (d) we plot the matrix χ where the two plots correspond to fidelities $F = 78\%$ and $F = 60\%$, respectively.

Conclusions. — We demonstrated spin-current mediated resonant coupling between a Majorana qubit and a mechanical resonator. The coupling can manifest itself in a shift of the mechanical resonant frequency, Rabi oscillations, coherent state transfer and Majorana qubit/resonator entanglement. In addition, the spin-current mediated coupling can facilitate both control of Majorana zero modes in a quantum wire and transfer of quantum information between topological and conventional qubits. The possibility to control the coupling and non-dissipative spin currents in the spin-transistor type architecture paves the way for applications in novel electronic devices. Our predictions can be tested by employing the magnetic resonance force microscopy techniques.

We are grateful to Leonid Pryadko for multiple helpful discussions. AAK and AD were supported in part by the U.S. Army Research Office under Grant No. W911NF-11-1-0027, and by the NSF under Grant No. 1018935. KS was supported in part by the DARPA-QuEST program and by the NSF under Grant DMR-0748925.

I. SUPPLEMENTARY MATERIAL

In this supplementary material, we present more details on analytical solutions for the edge states in topological (T) and non-topological (N) wires, and further apply these results to T-N-T and N-T-N setups.

A. General solutions

We consider the BdG Hamiltonian:

$$H = k^2 \hat{\tau}^z + uk \hat{\tau}^z \hat{\sigma}^z - \mu \hat{\tau}^z + \Delta (\cos \phi \hat{\tau}^x - \sin \phi \hat{\tau}^y) - b \hat{\sigma}^z + B (\cos \theta \hat{\sigma}^x - \sin \theta \hat{\sigma}^y), \quad (8)$$

where we use the Nambu spinor basis $\Psi^T = (\psi_\uparrow, \psi_\downarrow, \psi_\downarrow^\dagger, -\psi_\uparrow^\dagger)$ and the Pauli matrices σ^i and τ^i describe the spin and particle-hole sectors, respectively. The Hamiltonian in Eq. (2) is written in dimensionless units where $u = \alpha_{\text{so}}/t_0 a$ is the dimensionless strength of spin-orbit interaction, μ is the chemical potential, $\Delta e^{i\phi}$ is the superconducting pairing, b is the magnetic field along the z -direction and B is the magnetic field in the xy -plane. The energy unit is $t_0 = \hbar/2m^*a^2$, α_{so} is the Rashba spin-orbit coupling and the unit of length a is the lattice spacing for the tight binding representation of the Hamiltonian. It is convenient to transform Eq. (8) into the following non-Hermitian form:

$$G = V^\dagger U^\dagger H U V \tau^z \hat{\sigma}^z,$$

explicitly

$$G = k^2 \hat{\sigma}^z + uk - (b \hat{\tau}^z + i \Delta \hat{\tau}^x) - (\mu \hat{\sigma}^z + i B \hat{\sigma}^x). \quad (9)$$

The eigen solutions of the matrix G correspond to the following eigen values:

$$E_i = ku \pm \left[\sqrt{(\mu - k^2)^2 - B^2} \pm \sqrt{b^2 - \Delta^2} \right]. \quad (10)$$

By taking the product of eigen values in Eq. (10) one can obtain the condition on a gapped phase, i.e. whenever there are real solutions of equation:

$$\left\{ k^2 u^2 - \left[\sqrt{(\mu - k^2)^2 - B^2} + \sqrt{b^2 - \Delta^2} \right] \right\} \times \left\{ k^2 u^2 - \left[\sqrt{(\mu - k^2)^2 - B^2} - \sqrt{b^2 - \Delta^2} \right] \right\} = 0, \quad (11)$$

the wire is in a gapless phase. When there are no real solutions of Eq. (11) the wire is in a gapped case. Here, we limit our consideration by condition $\Delta^2 > b^2$ in which case the Hamiltonian (8) is always gapped with two phases, topological (T) for $\Delta^2 - b^2 < B^2 - \mu^2$ and non-topological (N) for $\Delta^2 - b^2 > B^2 - \mu^2$, being separated by a quantum phase transition at $\Delta^2 - b^2 = B^2 - \mu^2$.

In the gapped phase, we solve Eq. (11) by substituting $k = -i\kappa$ and finding 4-component solution to the Hamiltonian (8) in the form $\Psi(x) = e^{\kappa x} \Psi(\kappa)$ where we arrive at four solutions with $\Re(\kappa) > 0$ and at four solutions with $\Re(\kappa) < 0$. The general form of the corresponding non-normalized eigen vectors becomes:

$$\Psi(x)^T = e^{\kappa x} \left(b \pm \sqrt{b^2 - \Delta^2}, i\Delta \right) \otimes \left(\mu + \kappa^2 \pm \sqrt{(\mu + \kappa^2)^2 - B^2}, iB \right).$$

B. Solutions for topological and non-topological regions

In order to avoid very complicated analytical expressions, in our discussion we assume $b = 0$. We arrive at four solutions for the topological region, $\kappa_{-1}^> = \kappa_1^t$, $\kappa_{-2}^> = \kappa_2^t > 0$, $\kappa_{-3}^> = \kappa_1^{t*}$, $\kappa_{+4}^> = \kappa_3^t > 0$, for $\Re(\kappa) > 0$ and four solutions, $\kappa_{-1}^< = -\kappa_3^t$, $\kappa_{+2}^< = -\kappa_1^{t*}$, $\kappa_{+3}^< = -\kappa_2^t$, $\kappa_{+4}^< = -\kappa_1^t$, for $\Re(\kappa) < 0$ where κ_1^t , κ_1^{t*} and κ_2^t corresponds to equations $\pm \sqrt{B^2 - (\kappa^2 + \mu)^2} = \Delta + u\kappa$ and κ_3^t corresponds to equations $\pm \sqrt{B^2 - (\kappa^2 + \mu)^2} = \Delta - u\kappa$. General 4-component unnormalized topological solutions take the form:

$$\Psi_i^t(x) = e^{x\kappa_i^{>(<)}} V U \tau^z \sigma^z \begin{pmatrix} \mp i(\mu + k^2) - \Delta \mp u\kappa_i^{>(<)} \\ B \\ -i(\mu + k^2) \mp \Delta - u\kappa_i^{>(<)} \\ B \end{pmatrix}, \quad (12)$$

where $V = e^{-i\frac{\pi}{4}\tau^z\sigma^z}$ and $U = e^{i\frac{\phi}{2}\tau^z} \otimes e^{i\frac{\theta}{2}\sigma^z}$.

In the non-topological region we assume that $B = 0$, thus arriving at four solutions, $\kappa_1^> = \kappa_1^n$, $\kappa_2^> = \kappa_1^{n*}$, $\kappa_3^> = \kappa_2^n$, $\kappa_4^> = \kappa_2^{n*}$, for $\Re(\kappa) > 0$ and at four solutions, $\kappa_1^< = -\kappa_2^{n*}$, $\kappa_2^< = -\kappa_1^n$, $\kappa_3^< = -\kappa_1^{n*}$, $\kappa_4^< = -\kappa_2^n$, for $\Re(\kappa) < 0$ where $\kappa_1^n = iu/2 + i\sqrt{\mu + u^2/4 - i\Delta}$ and $\kappa_2^n = iu/2 - i\sqrt{\mu + u^2/4 + i\Delta}$. The 4-component non-normalized solutions can be expressed in the following form:

$$\Psi_i^n(x) = e^{x\kappa_i^{<(>)}} V U \tau^z \sigma^z \Psi_i, \quad (13)$$

where $\Psi_1 = (0, 1, 0, 1)^T$, $\Psi_2 = (1, 0, 1, 0)^T$, $\Psi_3 = (0, -1, 0, 1)^T$ and $\Psi_4 = (-1, 0, 1, 0)^T$.

C. Hybridization of Majorana modes and spin currents in T-N-T wire

We consider a semiconductor wire that has two infinite T-regions and a finite N-region. We introduce parameters $\{\Delta_l, B_l, \mu_l, \theta_l\}$ for the left T-regions, $\{\Delta_m, \mu_m\}$ for the middle N-region and $\{\Delta_r, B_r, \mu_r, \theta_r\}$ for the right T-region (see Fig. 2, main text). The phase of superconducting pairing is assumed constant (i.e. $\phi = 0$) throughout the wire. The solutions in Eqs. (12) and (13) and their derivatives are continuous at the boundary between the T and N-regions leading to unique solution for the Majorana mode. We denote such solutions as $|\psi_L\rangle = e^{i\frac{\theta_l}{2}\hat{\sigma}^z} |\psi_L^0\rangle$ for the left Majorana edge and as $|\psi_R\rangle = e^{i\frac{\theta_r}{2}\hat{\sigma}^z} |\psi_R^0\rangle$ for the right Majorana edge (see Fig. 2 in the main text) where it is convenient to introduce solutions $|\psi_L^0\rangle$ and $|\psi_R^0\rangle$ corresponding to $\theta_l = \theta_r = 0$. When solutions for the left and right edges weakly overlap we can find the hybridization energy of Majorana modes and spin current at the N-T boundary by employing the low-

est order perturbation theory. For the hybridization energy we obtain:

$$E^n(\theta) \approx \frac{\left| \left\langle \psi_L^0 e^{-i\frac{\theta}{2}\hat{\sigma}^z} \left| H \right| e^{i\frac{\theta}{2}\hat{\sigma}^z} \psi_R^0 \right\rangle \right|}{\sqrt{\langle \psi_L^0 | \psi_L^0 \rangle \langle \psi_R^0 | \psi_R^0 \rangle}},$$

and for spin current we obtain:

$$j_s^z(x_R) = \frac{\Re \left\{ \left[\psi_L^\dagger(x_R) \mp i\psi_R^\dagger(x_R) \right] \hat{\sigma}^z \hat{v} \left[\psi_L(x_R) \pm i\psi_R(x_R) \right] \right\}}{2\sqrt{\langle \psi_L^0 | \psi_L^0 \rangle \langle \psi_R^0 | \psi_R^0 \rangle}},$$

where x_L and x_R are positions of the edge states, $\hat{v} = \partial \hat{H} / \partial p$, $\theta = \theta_r - \theta_l$ and $j_s^z(x_L) = j_s^z(x_R)$. Explicitly, we have

$$\left\langle \psi_L^0 e^{-i\frac{\theta}{2}\hat{\sigma}^z} \left| H \right| e^{i\frac{\theta}{2}\hat{\sigma}^z} \psi_R^0 \right\rangle = 2e^{-2\ell_n \Re(\kappa_2^m)} \left[L_R^1 R_L^{2*} (2\kappa_2^{m*} + iu) e^{\ell_n \kappa_2^m + \frac{i\theta}{2}} + L_R^2 R_L^{1*} (2\kappa_2^m - iu) e^{\ell_n \kappa_2^{m*} - \frac{i\theta}{2}} \right],$$

and spin current becomes:

$$j_s^z = \pm \frac{\partial E^n(\theta)}{\partial \theta},$$

which corresponds to the formula for the hybridization energy over the non-topological region in the main text:

$$\frac{E^n}{E_0^n} \approx e^{-\ell_n \Re(\kappa_2^m)} \cos \left[\frac{\theta}{2} + \Phi_0 + L \Im(\kappa_2^m) \right], \quad (14)$$

with

$$\Phi_0 = \arg [2\kappa_2^m - iu] + \frac{1}{2} \arg \left[L_R^2 R_L^{1*} / (L_R^1 R_L^{2*}) \right].$$

Here $|\psi_L^0\rangle$ and $|\psi_R^0\rangle$ can be written as

where x_L and x_R are positions of the edge states and

$$|\psi_L^0\rangle = \begin{cases} \sum_{i=1}^4 L_L^i \Psi_i^t(x); & x < x_L \\ \sum_{i=1}^4 R_L^i \Psi_i^n(x); & x > x_L \end{cases}, \quad (15)$$

$$|\psi_R^0\rangle = \begin{cases} \sum_{i=1}^4 L_R^i \Psi_i^n(x); & x < x_R \\ \sum_{i=1}^4 R_R^i \Psi_i^t(x); & x > x_R \end{cases}, \quad (16)$$

$$\begin{aligned} L_L^1 &= \frac{(i\Delta_1 - \mu_1)(\kappa_2^m - \kappa_2^{m*}) - \kappa_1^{1*}(\kappa_2^{m*} + \kappa_2^1)(u + i\kappa_2^1 + i\kappa_2^m) - i(\kappa_1^{1*})^2(\kappa_2^{m*} + \kappa_2^1) - \kappa_2^{m*}(\kappa_2^1 + \kappa_2^m)(u + i\kappa_2^1)}{(\kappa_1^1 - \kappa_1^{1*})(\kappa_1^1 - \kappa_2^1)(\kappa_1^{1*} + \kappa_1^1 + \kappa_2^1 + \kappa_2^m - iu)}, \\ L_L^2 &= \frac{-\kappa_1^{1*2}(\kappa_2^{m*} + \kappa_1^1) + i\kappa_1^{1*}(\kappa_2^{m*} + \kappa_1^1)(u + i\kappa_1^1 + i\kappa_2^m) + \kappa_2^{m*}(\kappa_1^1 + \kappa_2^m)(iu - \kappa_1^1) + (\Delta_1 + i\mu_1)(\kappa_2^m - \kappa_2^{m*})}{(\kappa_1^1 - \kappa_2^1)(\kappa_2^1 - \kappa_1^{1*})(\kappa_1^{1*} + \kappa_1^1 + \kappa_2^1 + \kappa_2^m - iu)}, \\ L_L^3 &= \frac{i\kappa_2^{m*}[(\kappa_1^1)^2 + \kappa_2^m(\kappa_1^1 + \kappa_2^1) + (\kappa_2^1)^2 - iu(\kappa_1^1 + \kappa_2^1 + \kappa_2^m)] + 2(\mu_1 - i\Delta_1)\Im(\kappa_2^m) + i\kappa_1^1\kappa_2^1(\kappa_1^1 + \kappa_2^1 + 2\Re(\kappa_2^m) - iu)}{2\Im(\kappa_1^1)(\kappa_1^{1*} - \kappa_2^1)(\kappa_1^{1*} + \kappa_1^1 + \kappa_2^1 + \kappa_2^m - iu)}, \\ R_L^2 &= \frac{(-|\kappa_1^1|^2(\kappa_2^{m*} + \kappa_2^1) + \kappa_2^{m*}(-i\Delta_1 + \mu_1 + i(\kappa_1^1 + \kappa_1^{1*})(u + i\kappa_2^1) + u^2 + i\kappa_2^1 u) - (\Delta_1 + i\mu_1)(i\kappa_2^1 + i(\kappa_1^1 + \kappa_1^{1*}) + u))}{B_1(i(\kappa_2^1 + \kappa_2^m) + i(\kappa_1^1 + \kappa_1^{1*}) + u)}, \\ L_L^4 &= R_L^3 = R_L^4 = L_R^3 = L_R^4 = R_R^4 = 0, \quad R_L^1 = L_R^2 = 1. \end{aligned} \quad (17)$$

The coefficients L_R^1 , R_R^1 , R_R^2 and R_R^3 can be obtained from R_L^2 , L_L^1 , L_L^2 and L_L^3 , respectively, by replacement $\kappa_1^1 \rightarrow -\kappa_1^1$, $\kappa_2^1 \rightarrow -\kappa_2^1$, $\kappa_2^m \rightarrow -\kappa_2^{m*}$, $\mu_1 \rightarrow \mu_r$, $B_1 \rightarrow B_r$ and $\Delta_1 \rightarrow \Delta_r$.

D. Hybridization of Majorana modes in N-T-N wire

We consider a semiconductor wire that has two infinite N-regions and a finite T-region. We introduce parame-

ters $\{\Delta_l, \mu_l\}$ for the left N-regions, $\{\Delta_m, B_m, \mu_m, \theta_m\}$ for the middle T-region and $\{\Delta_r, \mu_r\}$ for the right N-region (see Fig. 2, main text). The phase of superconducting pairing is assumed constant (i.e. $\phi = 0$) throughout the wire. The solutions in Eqs. (12) and (13) and their derivatives are continuous at the boundary between the T and N-regions leading to unique solution for the Majorana mode. We denote such solutions as $|\psi_L\rangle$ for the left Majorana edge and as $|\psi_R\rangle$ for the right Majorana edge (see Fig. 2 in the main text). Here, the angle θ_m

does not play any role. When solutions for the left and right edges weakly overlap we can find the hybridization energy of Majorana modes by employing the lowest order perturbation theory, i.e.

$$E^n \approx \frac{|\langle \psi_L | H | \psi_R \rangle|}{\sqrt{\langle \psi_L | \psi_L \rangle \langle \psi_R | \psi_R \rangle}},$$

Explicitly, we obtain

$$\begin{aligned} \langle \psi_L | H | \psi_R \rangle = & \frac{2}{B_m} e^{-L_t \kappa_1^m} R_R^{3*} \left(B_m R_L^1 \left(-\kappa_2^{r*} + \kappa_1^m - iu \right) + R_L^2 (\kappa_1^m - \kappa_2^r + iu) (\Delta_m + i((\kappa_1^m)^2 + \mu_m) + \kappa_1^m u) \right) \\ & + \frac{2}{B_m} e^{-L_t \kappa_1^{m*}} R_R^{1*} \left(B_m R_L^1 \left(\kappa_1^{m*} - \kappa_2^{r*} - iu \right) + R_L^2 (\kappa_1^{m*} - \kappa_2^r + iu) \left(\kappa_1^{m*} (u + i\kappa_1^{m*}) + \Delta_m + i\mu_m \right) \right) \\ & + \frac{2}{B_m} e^{-L_t \kappa_2^m} R_R^{2*} \left(B_m R_L^1 \left(-\kappa_2^{r*} + \kappa_2^m - iu \right) + R_L^2 (\kappa_2^m - \kappa_2^r + iu) (\Delta_m + i((\kappa_2^m)^2 + \mu_m) + \kappa_2^m u) \right), \end{aligned}$$

which corresponds to the formula for the hybridization energy over the topological region in the main text:

$$\frac{E^t}{E_0^t} \approx e^{-\ell_t \kappa_2^m} + |A_0| e^{-\ell_t \Re(\kappa_1^m)} \cos[\arg A_0 + \ell_t \Im(\kappa_1^m)], \quad (18)$$

with

$$A_0 = \frac{R_R^{1*} (B_m R_L^1 (\kappa_1^{m*} - \kappa_2^{r*} - iu) + R_L^2 (\kappa_1^{m*} - \kappa_2^r + iu) (\kappa_1^{m*} (u + i\kappa_1^{m*}) + \Delta_m + i\mu_m))}{R_R^{2*} (B_m R_L^1 (-\kappa_2^{r*} + \kappa_2^m - iu) + R_L^2 (\kappa_2^m - \kappa_2^r + iu) (\Delta_m + i((\kappa_2^m)^2 + \mu_m) + \kappa_2^m u))}.$$

Here we can take $|\psi_L\rangle = |\psi_R^0\rangle$ and $|\psi_R\rangle = |\psi_L^0\rangle$ in Eqs. (15) and (16) after replacement $x_L \leftrightarrow x_R$ since we can use localized solutions found in the previous section, i.e. we can use Eq. (17) for coefficients R_L^i and L_L^i after replacement of indices “m” \rightarrow “r” and “l” \rightarrow “m” and we can use coefficients R_R^i and L_R^i after replacement of indices “m” \rightarrow “l” and “r” \rightarrow “m”.

-
- [1] A. Y. Kitaev, Physics-Uspekhi **44**, 131 (2001).
 - [2] L. Fu and C. Kane, Phys. Rev. Lett. **100**, 096407 (2008).
 - [3] J. Nilsson, A. R. Akhmerov, and C. W. J. Beenakker, Phys. Rev. Lett. **101**, 120403 (2008).
 - [4] R. M. Lutchyn, J. D. Sau, and S. Das Sarma, Phys. Rev. Lett. **105**, 077001 (2010).
 - [5] Y. Oreg, G. Refael, and F. von Oppen, Phys. Rev. Lett. **105**, 177002 (2010).
 - [6] C. Nayak, S. H. Simon, A. Stern, M. Freedman, and S. Das Sarma, Rev. Mod. Phys. **80**, 1083 (2008).
 - [7] J. Alicea, Rep. Prog. Phys. **75**, 076501 (2012).
 - [8] C. Beenakker, Annu. Rev. Condens. Matter Phys. **4**, 113 (2013).
 - [9] V. Mourik, K. Zuo, S. M. Frolov, S. R. Plissard, E. P. A. M. Bakkers, and L. P. Kouwenhoven, Science **336**,

- 1003 (2012).
- [10] M. T. Deng, C. L. Yu, G. Y. Huang, M. Larsson, P. Caroff, and H. Q. Xu, Nano Letters **12**, 6414 (2012).
- [11] A. Das, Y. Ronen, Y. Most, Y. Oreg, M. Heiblum, and H. Shtrikman, Nat. Phys. **8**, 887 (2012).
- [12] L. P. Rokhinson, X. Liu, and J. K. Furdyna, Nat Phys **8**, 795 (2012).
- [13] D. Bagrets and A. Altland, Phys. Rev. Lett. **109**, 227005 (2012).
- [14] J. Liu, A. C. Potter, K. T. Law, and P. A. Lee, Phys. Rev. Lett. **109**, 267002 (2012).
- [15] D. I. Pikulin, J. P. Dahlhaus, M. Wimmer, H. Schomerus, and C. W. J. Beenakker, New Journal of Physics **14**, 125011 (2012).
- [16] E. J. H. Lee, X. Jiang, R. Aguado, G. Katsaros, C. M. Lieber, and S. De Franceschi, Phys. Rev. Lett. **109**, 186802 (2012).
- [17] S. Das Sarma, J. D. Sau, and T. D. Stanescu, Phys. Rev. B **86**, 220506 (2012).
- [18] A. D. K. Finck, D. J. Van Harlingen, P. K. Mohseni, K. Jung, and X. Li, Phys. Rev. Lett. **110**, 126406 (2013).
- [19] J. Alicea, Y. Oreg, G. Refael, F. von Oppen, and M. P. A. Fisher, Nature Physics **7**, 412 (2011).
- [20] J. C. Y. Teo and C. L. Kane, Phys. Rev. Lett. **104**, 046401 (2010).
- [21] J. D. Sau, S. Tewari, and S. Das Sarma, Phys. Rev. A **82**, 052322 (2010).

- [22] J. D. Sau, D. J. Clarke, and S. Tewari, Phys. Rev. B **84**, 094505 (2011).
- [23] K. Flensberg, Phys. Rev. Lett. **106**, 090503 (2011).
- [24] B. I. Halperin, Y. Oreg, A. Stern, G. Refael, J. Alicea, and F. von Oppen, Phys. Rev. B **85**, 144501 (2012).
- [25] A. Romito, J. Alicea, G. Refael, and F. von Oppen, Phys. Rev. B **85**, 020502 (2012).
- [26] F. Hassler, A. R. Akhmerov, C.-Y. Hou, and C. W. J. Beenakker, New J. Phys. **12**, 125002 (2010).
- [27] L. Jiang, C. L. Kane, and J. Preskill, Phys. Rev. Lett. **106**, 130504 (2011).
- [28] P. Bonderson and R. M. Lutchyn, Phys. Rev. Lett. **106**, 130505 (2011).
- [29] F. Hassler, A. R. Akhmerov, and C. W. J. Beenakker, New J. Phys. **13**, 095004 (2011).
- [30] D. Pekker, C.-Y. Hou, V. Manucharyan, and E. Demler, arXiv:1301.3161 (unpublished).
- [31] L. Fu and C. L. Kane, Phys. Rev. B **79**, 161408 (2009).
- [32] L. Jiang, D. Pekker, J. Alicea, G. Refael, Y. Oreg, and F. von Oppen, Phys. Rev. Lett. **107**, 236401 (2011).
- [33] Q. Meng, V. Shivamoggi, T. L. Hughes, M. J. Gilbert, and S. Vishveshwara, Phys. Rev. B **86**, 165110 (2012).
- [34] L. Jiang, D. Pekker, J. Alicea, G. Refael, Y. Oreg, A. Brataas, and F. von Oppen, Phys. Rev. B **87**, 075438 (2013).
- [35] P. Kotetes, A. Shnirman, and G. Schön, arXiv:1207.2691 (unpublished).
- [36] S. Groblacher, K. Hammerer, M. R. Vanner, and M. Aspelmeyer, Nature (2009).
- [37] O. D. O'Connell, M. Hofheinz, M. Ansmann, R. C. Bialczak, M. Lenander, E. Lucero, M. Neeley, D. Sank, H. Wang, M. Weides, et al., Nature **464**, 697 (2010).
- [38] A. A. Kovalev, L. X. Hayden, G. E. W. Bauer, and Y. Tserkovnyak, Phys. Rev. Lett. **106**, 147203 (2011).
- [39] D. A. Garanin and E. M. Chudnovsky, Phys. Rev. X **1**, 011005 (2011).
- [40] L. Berger, Phys. Rev. B **54**, 9353 (1996).
- [41] J. Slonczewski, Journal of Magnetism and Magnetic Materials **159**, L1 (1996).
- [42] A. A. Kovalev, G. E. W. Bauer, and A. Brataas, Phys. Rev. B **75**, 014430 (2007).
- [43] G. Zolfagharkhani, A. Gaidarzhy, P. Degiovanni, S. Kettemann, P. Fulde, and P. Mohanty, Nat Nano **3**, 720 (2008).
- [44] S. Datta and B. Das, Appl. Phys. Lett. **56**, 665 (1990).
- [45] S. Kolkowitz, A. C. Bleszynski Jayich, Q. P. Unterreithmeier, S. D. Bennett, P. Rabl, J. G. E. Harris, and M. D. Lukin, Science **335**, 1603 (2012).
- [46] See supplementary material for detailed expressions at <http://>.
- [47] M. Cheng, R. M. Lutchyn, V. Galitski, and S. Das Sarma, Phys. Rev. Lett. **103**, 107001 (2009).
- [48] J. D. Sau, S. Tewari, and S. Das Sarma, Phys. Rev. A **82**, 052322 (2010).
- [49] Y. N. Guo, J. Zou, M. Paladugu, H. Wang, Q. Gao, H. H. Tan, and C. Jagadish, Applied Physics Letters **89**, 231917 (pages 3) (2006).
- [50] B. Ganjipour, H. A. Nilsson, B. M. Borg, L.-E. Wernersson, L. Samuelson, H. Q. Xu, and C. Thelander, Applied Physics Letters **99**, 262104 (2011).
- [51] A. De and C. E. Pryor, Physical Review B **76**, 155321 (2007).
- [52] J. C. Meyer, M. Paillet, and S. Roth, Science **309**, 1539 (2005).
- [53] J. Johansson, P. Nation, and F. Nori, Comput. Phys. Commun. **183**, 1760 (2012).
- [54] G. Goldstein and C. Chamon, Phys. Rev. B **84**, 205109 (2011).
- [55] D. Rainis and D. Loss, Phys. Rev. B **85**, 174533 (2012).
- [56] J. D. Teufel, T. Donner, D. Li, J. W. Harlow, M. S. Allman, K. Cicak, A. J. Sirois, J. D. Whittaker, K. W. Lehnert, and R. W. Simmonds, Nature **475**, 359 (2011).